Sensitivity of Caspian sea-ice to air temperature

Helen Tamura-Wicks [a*] Ralf Toumi [a] and W. Paul Budgell [ab]

[a]Space and Atmospheric Physics Group, Imperial College London, UK

[b]Institute of Marine Research, Bergen, Norway

[*]Correspondence to: H. Tamura-Wicks, Space and Atmospheric Physics Group, Blackett Laboratory, Imperial College London, London, SW7 2AZ, UK. E-mail: helen.tamura-wicks07@imperial.ac.uk

Caspian sea ice concentration from satellite passive microwave data and surface daily air temperatures are analysed from 1978 to 2009. Relationships between mean winter air temperatures, cumulative freezing degree days (CFDD) and the sum of daily ice area (cumulative ice area) are found. These show that mean monthly air temperatures of less than 5.5 to 9.5°C, and a minimum CFDD of 3.6±11.2°C, is required for ice formation in the Northern Caspian. Examination of climate projections from multi-model ensembles of monthly mean air temperatures suggest that the Northern Caspian may be largely ice-free by 2100 for the highest emission scenario. An ocean-ice-atmosphere model of the Caspian shows weak sensitivities of the minimum CFDD to varied sea ice albedo and ice compressive strength. Sea level decline is found to reduce the minimum CFDD as well as promote the formation of higher concentration or "closed ice". Copyright © 0000 Royal Meteorological Society

Key Words: Caspian sea ice; air temperature; cumulative freezing degree days; regional model sensitivity; albedo; compressive strength; sea level; CMIP5 projection

Received . . .

Citation: . . .

1. Introduction

Located between Iran, Azerbaijan, Turkmenistan, Kazakhstan and Russia is perhaps one of the world's most

This article has been accepted for publication and undergone full peer review but has not been through the copyediting, typesetting, pagination and proofreading process, which may lead to differences between this version and the Version of Record. Please cite this article as doi: 10.1002/qj.2592

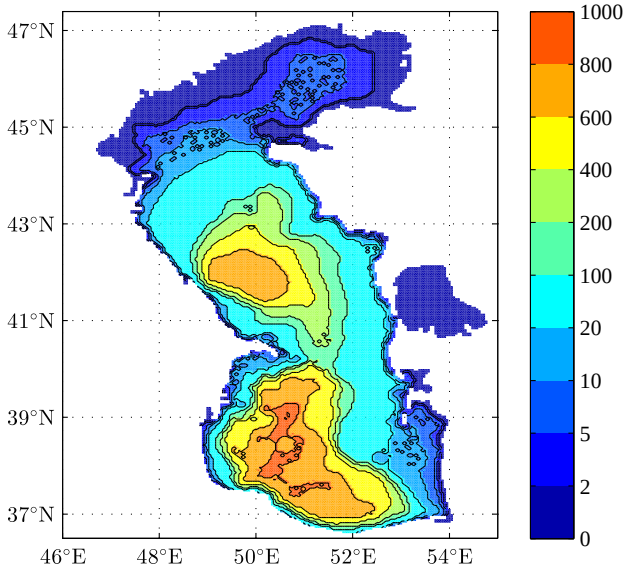

Figure 1. Bathymetry of the Caspian Sea in metres. The sea consists of the Northern, Middle and Southern Caspian basins. The Northern Caspian is characterised by its shallow depth of 20m or less, while the Middle and Southern Caspian both contain deep troughs and are separated by a saddle at approximately 100m depth.

unique water-bodies; the Caspian Sea. It is the largest totally enclosed sea on Earth (Ibrayev *et al.* 2009) and one of the most sensitive. The Northern Caspian, characterised by its shallow depth of 20m or less (Ibrayev *et al.* 2009) as shown in Figure 1, along with the Bohai Sea in China, the Sea of Okhotsk near Japan and the Great Lakes, lies on the southernmost boundary within the Northern Hemisphere where sea or lake ice forms (Kouraev *et al.* 2004; Barry and Gan 2011). Sea ice located this far south experience sensitivities in seasonal and inter-annual fluctuations in ice production larger than those in the northern regions. (Falk-Petersen *et al.* 2000).

Historical observations show that sea ice is typically present in the Northern Caspian from mid-November to March. However, these timings for ice appearance and disappearance may vary by up to a month depending on the severity of the winter (Kouraev *et al.* 2004). Maximum ice coverage for a particular winter is also highly variable - this sensitivity of sea ice may be of interest in the longer term as it can potentially act as an early indicator of large-scale climate change (Kouraev *et al.* 2004). Future ice conditions are also of concern to various industries, such as fisheries, transportation and oil companies operating in the Northern Caspian (Rodionov 1994). Any future reduction in ice cover may negatively affect species already listed as vulnerable, such as the Caspian seal, as was seen when there was reduced ice cover in 2000 (Kouraev *et al.* 2004).

Past studies on Caspian sea ice include investigations of sea ice ridging, rafting, ice pile-up and hummocks through modelling and observations (Bailey *et al.* 2010; Klyachkin 2011; Andreev and Ivanov 2012; Frolov *et al.* 2009). Ocean and atmospheric variables of the Caspian have also been modelled with sea ice used as a boundary condition (Syed *et al.* 2010; Semenov *et al.* 2012; Kitazawa and Yang 2012; Ibrayev *et al.* 2009). However, studies on the sensitivities of the Caspian are limited in number and mostly deal with changes in sea level fluctuations as opposed to ice conditions (Renssen *et al.* 2007; Elguindi and Giorgi 2007, 2006).

Nevertheless, sensitivity studies of sea ice coverage have been carried out in regions similar to the Caspian. Correlations were found between air temperature and sea ice coverage in the Great Lakes and Bohai Sea, which are at similar latitudes as the Caspian (Su *et al.* 2012; Assel 1980; Assel *et al.* 1996). Air temperature was converted to cumulative freezing degree days (CFDD) for these analyses, which is effectively a measure of both how cold the air temperature is and for how long. The sensitivity of Caspian sea ice coverage to air temperature or CFDD are therefore examined here for the first time.

Sea ice conditions are also known to be affected by its albedo, compressive strength and sea level. It is thought that changes in surface albedo has a positive feedback on the air temperature (Curry *et al.* 1995), and affects the sea ice coverage in return. For the compressive strength, which is a measure of the compactness of the ice, its coverage may be affected by differences in the amount of deformation the ice may undergo (Hibler III and Walsh 1982; Hibler III 1979). As for the sea level, its recent decline in the Aral Sea is thought to affect its heat storage capacity, which appears to modify its ice conditions (Kouraev *et al.* 2004). A regional ocean-ice-atmosphere model is therefore used to investigate

the sensitivity of sea ice coverage in the Caspian to air temperature, to a range of parameters.

2. Methods

2.1. *Sensitivity of ice to air temperature*

2.1.1. *Definitions*

Ice conditions in the Northern Caspian are known to be dependant on winter severity (Kouraev *et al.* 2004). Correlations between monthly mean air temperatures and ice area were therefore examined here for the first time in detail. In quantifying the ice area in the Northern Caspian, the sum of daily sea ice area (cumulative area) over a given time period was chosen as a metric, as accumulating daily ice coverage has been suggested to a be a more robust measure than maximal ice coverage alone in describing the severity of a given winter (Kouraev *et al.* 2004). The Northern Caspian was defined as the region to the north of 44°N for the purposes of this study, which roughly corresponds to where a depth of 20m separates the Northern basin to the Middle Caspian. In computing the daily sea ice area, a sea ice concentration of 15% was taken as a threshold to determine whether a particular grid point can be considered to be covered by ice (Gloersen *et al.* 1992; Parkinson *et al.* 1999). The area of the ice-covered grid cells are referred to as sea ice extent. Multiplying the ice extent by its ice concentration at each grid point will then give ice area at that grid point. Monthly correlations between mean air temperature and cumulative area were calculated from November to March, from the first day of the month to when daily ice area reaches its monthly maximum.

Daily correlations between air temperature and sea ice were also examined. The amount of sea ice produced in a region is related to how cold and how long the air temperature has been below the freezing temperature of the sea, and can be quantified by calculating cumulative freezing degree days (CFDD) (Assel 1980; Business 2002). This is typically defined as the sum of the differences in mean daily surface air temperatures and the freezing temperature of the sea over a given period, as described by equation 1;

$$CFDD = \int_{t=d_s}^{t=d_e} (T_f - T_a)dt \qquad (1)$$
$$when \qquad T_a(t) <= T_f$$

where T_f is the freezing temperature of the sea, T_a is the mean daily 2m surface air temperature and t is time in units of days over which CFDD is analysed, beginning and ending on date d_s and d_e respectively. The freezing temperature was determined by $T_f = -0.054S$, where S is the salinity of the water-body in practical salinity units. Given a mean salinity of 11.2psu in the Northern Caspian, the freezing temperature was set to -0.60°C. The CFDD was then correlated to cumulative ice area.

2.1.2. *Data*

Satellite observations of sea ice and air temperature data from stations were used to empirically examine the correlation of sea ice conditions to air temperature. Reprocessed sea ice concentrations derived from SMMR and SSM/I observations (EUMETSAT Ocean and Sea Ice Satellite Application Facility 2011) were used for computing the sea ice area. This has a spatial resolution of 12.5km and is available daily from October 1978 to June 2009. Daily mean 2m air temperatures from stations along the coast of the Northern Caspian were obtained from the National Climatic Data Centre (Klein Tank *et al.* 2002). Daily mean 2m temperatures were averaged for four sites surrounding the Northern Caspian (Fort Shevchenko, Kaspiyskiy, Tyuleniy Ostrov and Atyrau, shown in Figure 2) to create an index to describe air temperatures over the Northern Caspian.

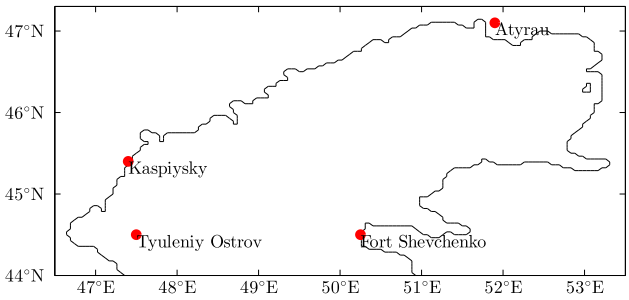

Figure 2. Station locations used for sensitivity analysis. Fort Shevchenko: 44.6°N, 50.3°E, Kaspiyskiy: 45.4°N, 47.4°E, Atyrau: 47.1°N, 51.9°E, Tyuleniy Ostrov: 44.5°N, 47.5°E

2.2. Model Sensitivities

2.2.1. Model Description

A coupled ice-ocean model forced by a regional atmospheric model was set up to simulate the period 1 January 2006 to 1 May 2009 with three-hourly output intervals.

The atmospheric model used was the Weather Research and Forecasting model (WRF), which is a three-dimensional, non-hydrostatic, quasi-compressible atmospheric model that uses sigma coordinates to simulate meso- and micro- scale atmospheric variables (Skamarock *et al.* 2008). The model domain has a horizontal resolution of 36km and 36 vertical levels, spanning 20-60°N and 0-80°E. It contains two nested grids within it, with 12 and 4km horizontal resolution. It is forced at the boundary by the ERA-Interim dataset, which is a reanalysis product produced by the European Centre for Medium-Range Weather Forecasts (ECMWF) (Dee *et al.* 2011). ERA-I was also used to initialise the simulation. Six-hourly sea ice coverage is taken into account as part of the boundary forcing in WRF, for which fractional sea ice coverage from SSM/I observations were used between November and May during each year of the simulation.

Atmospheric fields from the innermost WRF nest were then applied to the Regional Ocean Modelling System (ROMS) with 4km horizontal resolution and 32 vertical levels. ROMS is a three-dimensional, free-surface, sigma-coordinate numerical model. In order to model the dynamics, ROMS solves the Reynolds-averaged Navier-Stokes equations using the hydrostatic and Boussinesq assumptions (Haidvogel *et al.* 2000; Shchepetkin and McWilliams 2005). 10m wind speeds, precipitation, 2m specific humidity, downward longwave and shortwave radiation, sea surface pressure and 2m air temperature from WRF were used to force ROMS at the sea surface. River discharge data from the Global River Discharge Database (Vörösmarty *et al.* 1998) were used as river forcing in ROMS for the Volga, Ural, Kura, Samur, Sulak and Terek rivers at their respective outlets to the Caspian. In addition, ROMS contains a sea ice model which is coupled to the ocean. This uses a one layer snow and ice thermodynamics (Mellor and Kantha 1989) combined with the use of elastic-viscous-plastic rheology (Hunke and Dukowicz 1997). This dynamic-thermodynamic sea ice model is documented by Røed and Debernard (2004). The coupled ice-ocean version of ROMS has been successfully applied to the Barents Sea (Budgell 2005) and the Bering Sea (Danielson *et al.* 2011). To account for the effects of the shallow bathymetry in the northern basin on ice drift and the presence of fast ice, an empirical treatment is applied in which, if the water column thickness below the ice cover is less than 0.5 m, ice drift is zero. If the water column thickness is greater than 1.5 metres, ice is free to drift. If the water column thickness is between 0.5 and 1.5 m, the ice drift retardation is linearly interpolated between these two end points.

The advection of ice, and therefore its coverage, is partly determined by the pressure within the ice and is related to the sea ice compressive strength parameter through equation 2;

$$P = P^* h\, e^{-C(1-A)} \tag{2}$$

where P is the internal ice pressure, h is the thickness of ice in metres, A is the fractional coverage of sea ice (between 0 an 1) and P^* (sea ice compressive strength parameter), C are empirically determined constants (Hibler III 1979). The elastic-viscous-plastic rheology

employed in the model is set up so that sea ice has little resistance to tensile stress, but is highly resistant to compression during convergence. *P** is thought to vary with ice thickness, where $P^* \propto h^n$, and the constant *n* remains one of the largest uncertainties ($\frac{1}{2} \leq n \leq 2$) (Thomas and Dieckmann 2008).

2.2.2. *Model Experiments*

Table 1 lists the model sensitivity experiments. Examination of remote sensing data (MOD10A1 dataset (Hall *et al.* 2006)) reveals that albedo of bare ice, which is likely to be present during the first week when ice is formed in the basin, was around 0.43. On the other hand, snow-covered ice which is prevalent during mid-winter, has an albedo of approximately 0.80 (Farmer and Cook 2013). These two values were therefore used in both WRF and ROMS to conduct the albedo experiment to capture the entire range of variabilities in ice albedo.

As compressive strength is a variable with one of the largest unknowns associated with it (Thomas and Dieckmann 2008), many different values for it have been tested in models against observations over the years. Based on compressive strength parameters used in those studies (Hibler III and Walsh 1982; Kreyscher *et al.* 2000), P* of 1000, 5000 and 27500 Nm^{-2} were used as a test case for the sensitivities in the Caspian.

As for the sea level, there have been significant changes during the 20th century alone - a rapid 1.7m drop in sea level was observed in the 1930s, followed by a rise of 2.5m in the 1980s (Arpe *et al.* 2000). A 2m decrease in sea level was therefore assumed for the sensitivity study.

3. Results

3.1. *Sensitivity of ice to air temperatures*

3.1.1. *Monthly Correlations*

Observed monthly mean index temperatures and observed cumulative ice area were compared with each other (Figure3). The R^2 were 0.72, 0.79, 0.63, 0.77 and 0.83 from November to March, suggesting a linear relationship (these were 0.60, 0.71, 0.53, 0.75 and 0.75 for temperatures at Atyrau, for example, highlighting that the use of station index temperatures give better agreement as opposed to temperatures from individual stations). A linear fit suggests that critical monthly mean air temperatures of 8.2±0.3, 5.5±0.3, 9.5±1.0, 9.3±0.6 and 7.7±0.4°C from November to March are required for ice formation in the Northern Caspian.

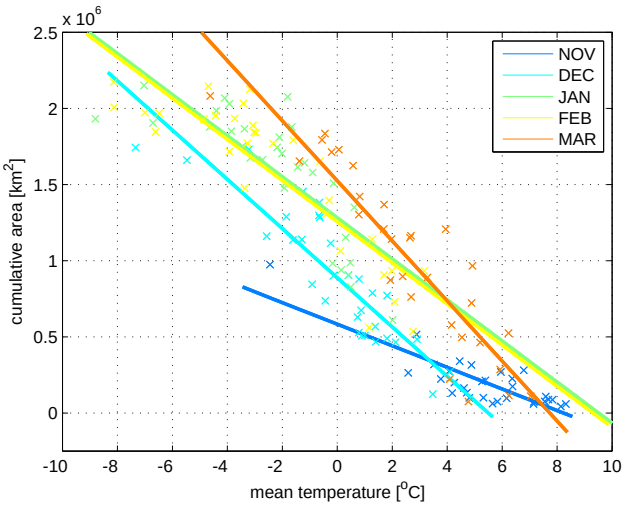

Figure 3. Monthly correlations between cumulative area and station mean index temperature. Each of the data points represent different years of observations, and the solid lines are the linear fit to those data points for different months.

The change in monthly mean temperature under climate change and the impact of this on sea ice is next explored. Multi-model mean projections in monthly mean air temperatures for the Northern Caspian were obtained from the fifth phase of the Climate Model Intercomparison Project (CMIP5) (Taylor *et al.* 2012), where 39 and 42 models were used to construct the ensemble mean for high (RCP8.5) and mid-range emission scenarios (RCP4.5) respectively. A ten-year running mean in monthly temperature projections were bias-adjusted to station index observations over 1978 to 2009 (base period). The adjusted monthly temperature projections and their corresponding critical monthly mean temperatures required for sea ice formation are shown for the high emission scenario (Figure4).

Experiment	WRF, ROMS sea ice albedo [%]	compressive strength [Nm^{-2}]	Sea level relative to datum [m]
Control	43	5000	0
Albedo	43	5000	0
Albedo	80	5000	0
compressive strength	43	1000	0
compressive strength	43	5000	0
compressive strength	43	27500	0
Sea level	43	5000	0
Sea level	43	5000	-2

Table 1. Model sensitivity experiments and variables used.

Changes in cumulative area for each month under 2100 conditions compared to the base period were determined from this, in conjunction with Figure3. In further quantifying the future changes in ice conditions, inter-annual variabilities in monthly mean index air temperatures were imposed on their temperature projections. The probability of a given month being ice-free was determined for 2100 conditions for both the high and mid-range emission scenarios, assuming that the standard deviations of the observed air temperatures do not vary in time, and that the inter-annual variabilities follow a Gaussian distribution. Table2 summarises these changes.

For the high-emission scenario, November is 89% likely to be ice-free under 2100 conditions, as well as December and March being ice-free with around 50% chance. Although January and February are not likely to be ice-free, the expected cumulative ice area in those months are about 40% less compared to the base period. Similar changes in ice conditions are expected under the midrange emission scenario, however to a lesser degree compared to the high emission scenario.

month	base [%]	2100 [%]	change in ΣA [%]
NOV	34	89 (37)	-100 (-76)
DEC	12	46 (16)	-95 (-51)
JAN	0	0 (0)	-41 (-26)
FEB	0	0 (0)	-42 (-25)
MAR	4	51 (17)	-100 (-54)

Table 2. Estimated changes in sea ice under 2100 conditions relative to 1978-2009 (base) period for a given month. The second column is the probability that a given month may be ice-free over the base period. The third column is the same but under 2100 conditions. The fourth column is the change in the expected cumulative area during a given month under 2100 conditions relative to the base period. For the third and fourth columns, the values contained in brackets are estimates for the projected 2100 conditions according to the RCP4.5 scenario, those that aren't are for the RCP8.5 scenario.

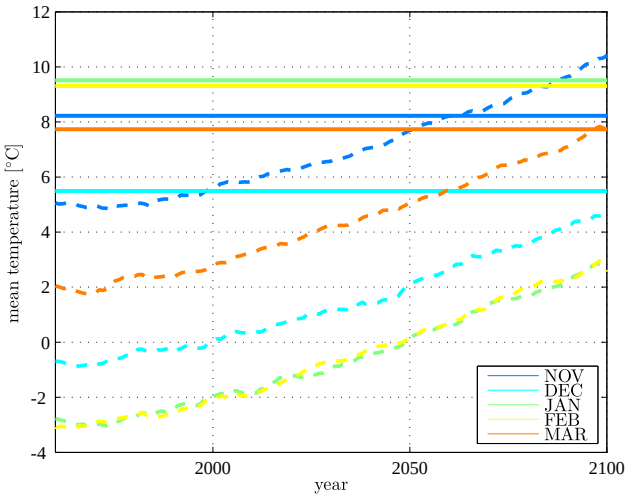

Figure 4. Comparison of future projections in station mean index temperatures from CMIP5 and their corresponding critical temperatures for every month between November and March. 10 year running means of the projection for the RCP8.5 scenario are depicted by the dotted lines. The critical temperatures over the winter months are denoted by solid lines.

3.1.2. *Daily Correlations*

Daily correlations between CFDD and cumulative ice area are shown in Figure5. Linear regression analysis on each winter observed gives an R^2 range of 0.81 to 0.99. A linear fit through each observed year gives a mean minimum CFDD of 3.6°C required for ice formation, with a standard deviation of 11.2°C.

3.2. *Model sensitivities*

Here the robustness of the dependence of cumulative ice area on CFDD to different ice properties and sea level are examined. The performance of the ocean-ice-atmosphere model is first evaluated.

3.2.1. *Validation of modelled ice cover*

The temporal evolution of ice extent and area are validated against SSM/I observations, in Figure 6. A lag in the timing

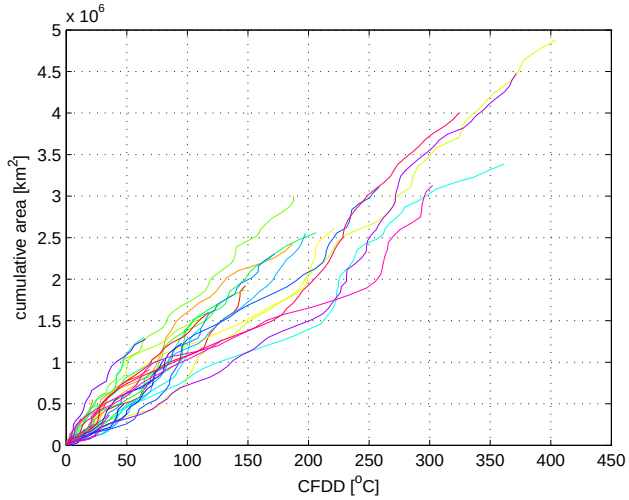

Figure 5. Daily correlations between cumulative ice area and CFDD. The different colours denote the daily evolution of these variables for the different winters observed.

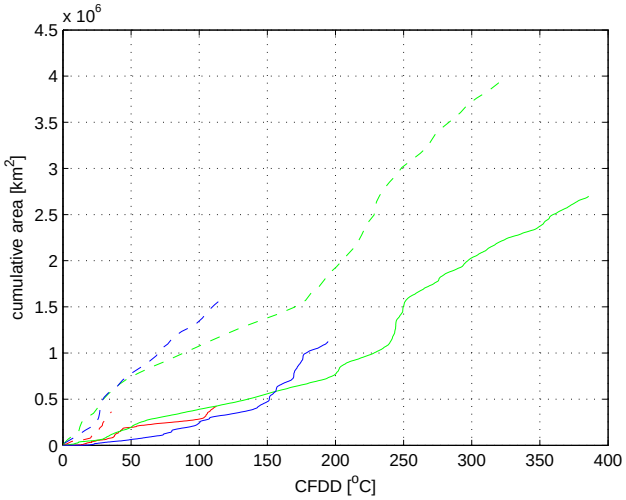

Figure 8. Daily evolution of cumulative ice area against CFDD for control model (solid line) and observations (dashed line). The red, green and blue lines are for the winters of 2007, 2008 and 2009, respectively.

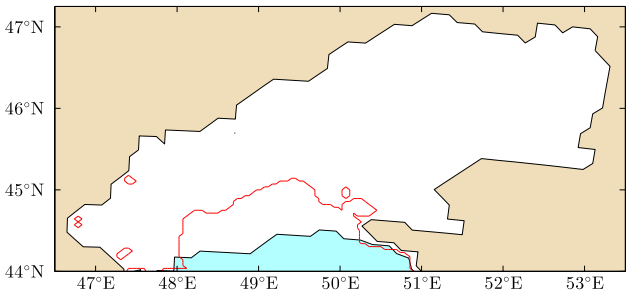

Figure 7. Map of observed three-year mean sea ice extent at its winter maxima. Areas covered in ice are denoted by white, land by brown and the sea by blue. Similarly, modelled ice contours are displayed in red.

of formation and melt of ice is present in the control model, for both ice area and extent. Maximum annual ice area over the three simulated years in the model control were 38.2% less that in observations, with modelled maximum annual ice extent at 6.5% less than observations. However, the overall temporal evolution of ice extent is emulated by the model control, with R^2 values of 0.23, 0.74 and 0.77 over the period displayed for the winter of 2007, 2008 and 2009 respectively. These were 0.22, 0.66 and 0.67 for ice area. In addition, Figure 7 shows the spatial distribution of mean ice extent at its annual maximum in the model control compared against SSM/I observations. Both the amount and spatial distribution of maximum ice extent agree well between the two.

Figure8 shows the daily evolution of cumulative area and CFDD in both the model and observations. R^2 values between model and observations for each of the years are 0.98, 0.99 and 0.89 for 2007, 2008 and 2009 respectively. Linear regression analysis of the observations show that a minimum CFDD of 5.0±2.9, 2.0±4.5 and -0.6±1.5°C were required for the onset of freezing. In the model, these were found to be 6.5±0.6, 29.0±2.0 and 27.9±1.7°C. The three-year mean minimum CFDD in the control model and observations are 21.1°C and 2.1°C respectively.

The observed maximal ice extent in the Northern Caspian and mean index air temperatures between November and March are shown in Figure 9. Both values in the model emulate those observed. Sea surface temperatures in ROMS over the Northern Caspian are 0.1 and 0.8°C colder in October and November respectively, compared to those in OSTIA (Stark *et al.* 2007) over the three years simulated.

3.2.2. *Sea ice albedo*

Daily correlations between cumulative area and CFDD are shown (Figure 10), along with a map of ice extent when it is at its winter maximum (Figure 11), for different sea ice albedo. A minimum CFDD of 6.5±0.6, 29.0±2.0 and 27.9±1.7°C were required for the onset of ice formation for the 0.43 albedo case for the winter of 2007, 2008 and 2009 respectively. For the 0.80 albedo case, a very similar minimum CFDD of 6.9±0.6, 31.0±2.1 and 30.0±1.8°C were found for the respective winters. In addition, there were no significant differences in the rate at which

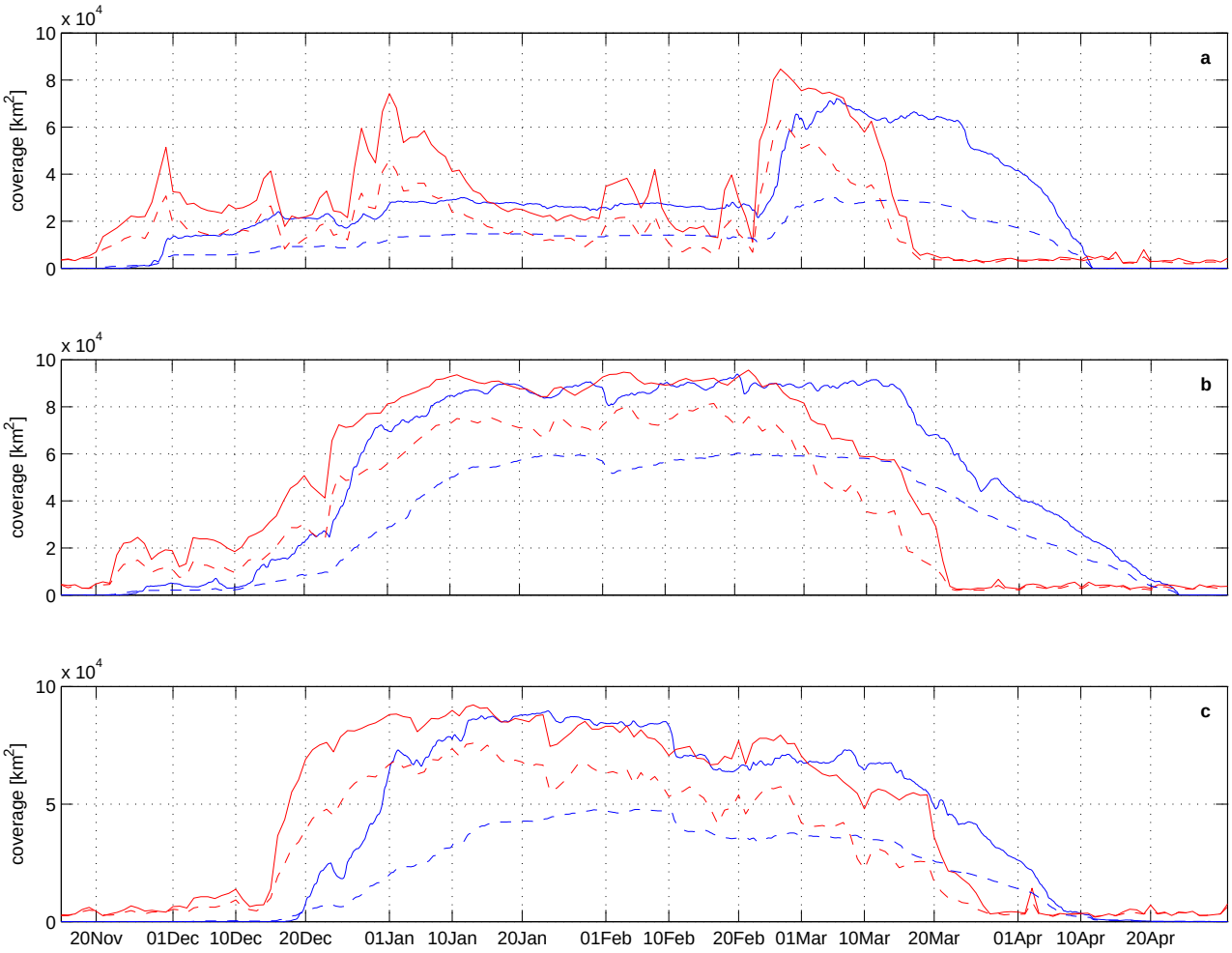

Figure 6. Comparison of daily sea ice extent for the control model (blue) and observations (red) in solid lines, and the same for sea ice area but with dotted lines. a,b and c are for the winter of 2007, 2008 and 2009, respectively.

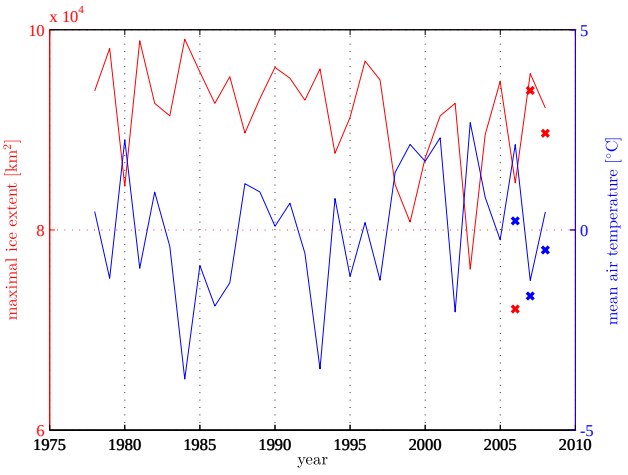

Figure 9. Ice extent at its annual maximum (red) and station mean index temperatures (blue), between November and March. Solid lines are those for observations and crosses are those for the control model.

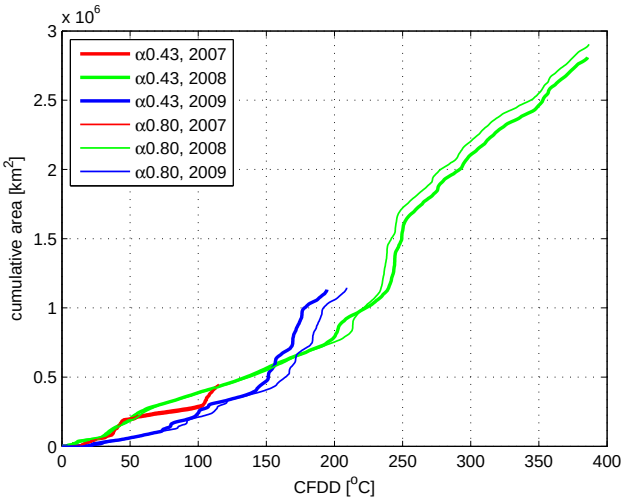

Figure 10. Daily correlations between cumulative ice area and CFDD for different ice albedo.

cumulative area evolved. The map of maximum ice extent do not show significant spatial differences in the distribution of ice between the two albedo simulations.

3.2.3. Compressive strength

Figure 12 and 13 respectively show the daily cumulative area correlations to CFDD along with the map of ice

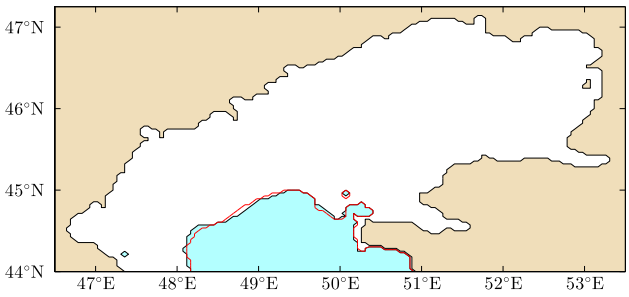

Figure 11. Map of three-year mean sea ice extent for when ice extents are at their winter maximum for albedo of 0.43. Areas covered in ice are denoted by white, land by brown and the sea by blue. Similarly, ice contours for ice albedo of 0.80 are displayed in red.

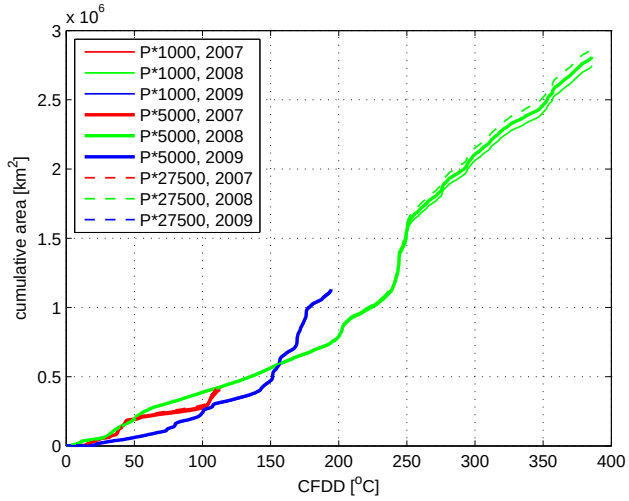

Figure 12. Daily correlations between cumulative ice area and CFDD for different compressive strengths.

extent at its winter maximum for a range of compressive strengths. A minimum CFDD of 6.2±0.6, 29.0±2.0 and 28.1±1.8°C were required for the onset of ice formation for the P*=1000Nm^{-2} case for the winter of 2007, 2008 and 2009 respectively. For the P*=27500Nm^{-2} case, a very similar minimum CFDD of 6.7±0.6, 29.4±2.0 and 28.0±1.7°C were found for the respective winters. As with the albedo sensitivity, there were no significant differences in the rate at which cumulative area evolved. No significant spatial differences were seen in the maximum ice extent across the different compressive strength simulations.

3.2.4. Sea level

Daily evolutions in cumulative area over the area to which the coastline retreats when sea level is reduced by 2m and CFDD are shown in Figure 14 for different sea levels. When sea level is at its datum, the minimum CFDD for the winter

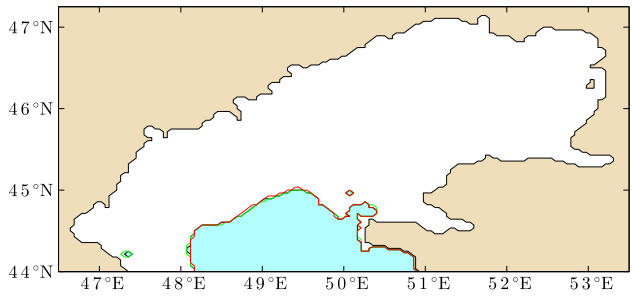

Figure 13. Map of three-year mean sea ice extent for when ice extents are at their winter maximum for compressive strength of 5000Nm^{-2}. Areas covered in ice are denoted by white, land by brown and the sea by blue. Similarly, ice contours for when compressive strengths are at 1000 and 27500Nm^{-2} are shown in green and red respectively.

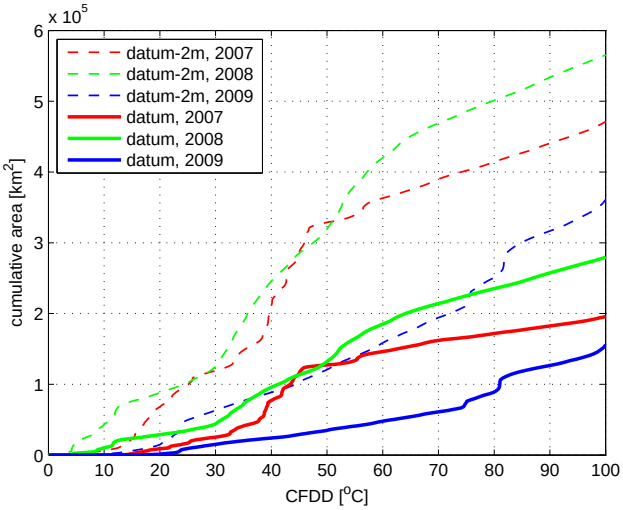

Figure 14. Daily correlations between cumulative ice area and CFDD for different sea levels.

of 2007, 2008 and 2009 were 10.9±0.6, 32.5±2.0 and 29.2±1.8°C respectively. When sea level was reduced by 2m, these decreased to 3.6±0.6, -4.6±0.9 and 13.4±0.6°C. Fluctuations in sea level modify the daily sensitivities of cumulative ice area to CFDD with some significance. Figure 15 shows a map of sea ice concentration when the ice extent is at its winter maximum. Formation of higher concentration ice was promoted when sea level was reduced. Sea ice of more than 50% fractional coverage is classified as closed ice (WMO 1970). Closed ice accounts for 53% of the total ice extent at its winter maximum when sea level is at its datum, but increases to 79% when sea level is reduced by 2m.

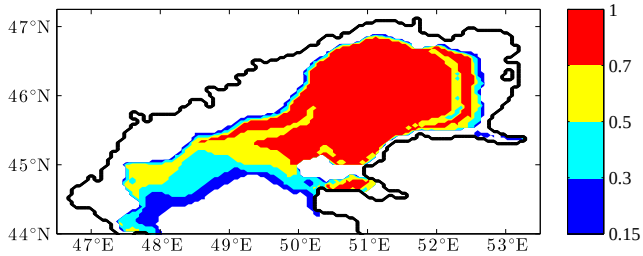

(a) datum-2m

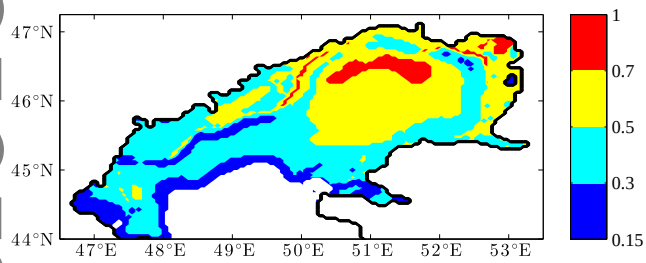

(b) datum

Figure 15. Map of three-year mean sea ice concentrations for when ice extents are at their winter maxima. The maps are for when sea level is 2m below datum (a) and when at its datum (b).

4. Discussion

Monthly and daily relationships computed using an index which is the mean of the air temperatures from the four different stations were found to have the highest correlations compared to any single station. The high correlation obtained for the index suggests that averaging the air temperatures at these stations is most representative of the Northern Caspian.

Good correlations were found in seasonal and daily relationships between air temperature, CFDD and cumulative ice area. However, there may be systematic errors. SSM/I based products tend to inadvertently classify coastal regions as ice covered due to land spillover effects (Cavalieri *et al.* 1999). Cumulative ice area may therefore be overestimated in the analyses, especially near the beginning of the ice season. This suggests that, in reality, the minimum CFDD may be higher compared to those derived in section 3.1. Similarly, the critical monthly mean temperatures may be lower in reality than those derived. Remote observations of Caspian sea ice are also available in the IMS (National Ice Centre 2008) and ARCLAKE (MacCallum and Merchant 2013) datasets, as well as local observations summarised by Kouraev et al (Kouraev *et al.* 2004). However, these were not suitable for computing cumulative ice area, as their ice concentration maps were either prone to cloud cover or were not available daily.

Observations show that temperatures are increasing at a rate of 4.5°C per century, however, CMIP5 projections show accelerated future warming. However, a loss of only $2.2x10^4 km^2$ of maximal ice extent per century can be inferred from observations. Simply extrapolating the current maximum ice extent would not result in a significant change in ice conditions by 2100. In contrast, the method of correlating air temperature with cumulative area presented here can be thought of as a more robust method in projecting future ice conditions. This would seem a good first approximation until global climate models can fully resolve the Caspian sea ice behaviour. As computing power increases, further work would be needed to establish the robustness of our projection with fully coupled high resolution projections of the area.

Under climate change, November, December and March are likely to be ice-free and the cumulative ice area may decrease by up to 40% in January and February by 2100 conditions (Table2). However, it is likely for these changes to be more amplified than those estimated, given the previously discussed systematic errors present in SSM/I observations. In addition, the response of ice formation to temperature changes appear to be suppressed in November compared to all other months, as this first month of ice-cover requires more cooling of the sea compared to subsequent months before reaching freezing point. As projected ice-free months increase, it is likely that this will have a knock-on effect on subsequent months where sea ice formation is further suppressed. This amplification effect is not included in our estimate.

The CFDD is a useful measure to characterise the relationship between maximum ice area and air temperature. The sum of CFDD were taken under freezing conditions for the Caspian in this study, however, in another approach, days when the air temperature becomes warmer than the freezing temperature (thawing degree days) are

included in the summation of CFDD over a continuous period. The CFDD is reset to zero once it reached a negative value (Business 2002; Su *et al.* 2012; Assel 1980; Assel *et al.* 1996). This method for calculating CFDD has also been compared against both cumulative area and daily ice areas for the Caspian, but it did not yield as good a correlation as the definition chosen here (Equation1). Taking into account of thawing degree days is likely to lead to lower daily correlations, as ice requires more heat flux in order to melt it than to form. Similarly, stopping the calculation of CFDD when ice area reaches its winter maximum did not significantly change the high correlations obtained, as opposed to stopping the computation when sea ice reaches, for example, 70% of its winter maximum. Additionally, ice extent and mean sea ice concentrations over the Northern Caspian, both cumulative and daily, were tested as a metric for describing ice conditions in the basin. These were found to not outperform the metrics used in this study.

Daily correlations in cumulative ice area and CFDD for the Northern Caspian appear to be comparable to those in other regions along similar latitudes as the Northern Caspian. Although thawing degree days have been taken into account in computing the CFDD in the Bohai Sea, the daily correlation between both ice area and CFDD evolution there are reported to be between 0.64 and 0.72 (Su *et al.* 2012), whereas here for the Northern Caspian it is much better at 0.93. Comparison of results to Lake Erie, one of the Great Lakes in North America, may also prove interesting especially as its depths are similar to that of the Northern Caspian. The mean depth of Lake Erie is 19m, with winter ice formation starting in its West Basin where the mean depth is 9m (Assel 1991). CFDDs there are also calculated by taking into account of thawing degree days. Comparison of Lake Erie ice charts to CFDD reveal that a minimum CFDD of 27°C is required before the onset of ice formation (Assel 1991), which is more than the minimum CFDD of 3.6±11.2°C for the Northern Caspian. However, given that the mean depth of the Northern Caspian being approximately 5m as opposed to 19m for Lake Erie, this is consistent with the finding of the sea level sensitivity experiment. In addition, future conditions in 2090 obtained from CGCM1 projections were used to estimate that Lake Erie could be ice-free for 96% of winters by 2090 (Lofgren *et al.* 2002). This is similar to the inferred projections for the Caspian in this study, which may also be largely ice-free by 2100.

Although the overall evolution of ice extent throughout the winter is reasonably simulated, model validations show a lag in individual events of sea ice formation and melt (Figure 6). This accounts for the low R^2 of 0.23 between the control model and observations for ice extent evolution over the winter of 2007, where there were successive events of extensive freezing and melting throughout the season, whereas a higher R^2 of 0.74 and 0.77 were seen during the winters of 2008 and 2009, where there was largely a single freezing event. The higher than observed minimum CFDD of 21.1°C required for ice formation in the model, as opposed to 2.1° according to observations, is consistent with the model's lag in ice formation. Although the same bias where ice formation lags is also present in other ROMS model studies, seasonal and inter-annual ice variabilities have been successfully validated against observations (Budgell 2005), indicating that the ice physics is largely represented by ROMS. Although it is not possible to quantitatively compare modelled ice thickness to those observed due to a lack of gridded datasets, modelled ice thickness appears to grow to those comparable to local observations summarised in Kouraev et al (Kouraev *et al.* 2004), which goes to some way in supporting the ice physics representation of ROMS. Disparities in surface fluxes in WRF, and therefore the ROMS forcings, could potentially contribute to the lag in modelled ice formation. Maykut (Maykut 1978) shows that differences in ice thickness in the central Arctic results in large disparities in surface fluxes, which scales with ocean-atmosphere temperature differences. Based on his calculations, any variations in prescribed ice thickness in WRF would result in negligible

differences in surface fluxes, for the ocean-atmosphere temperature differences seen over the Northern Caspian. In addition, the daily evolution of CFDD and cumulative area in the control model emulate those observed with high correlations in the range of 0.89 to 0.99. This suggests that the behaviour of sea ice evolution in response to CFDD is well modelled. Although the observed cumulative area is approximately two to four times those modelled, at 100°C CFDD for example, this was contained to within a factor of two when compared using cumulative extent. Using extent as a metric, as opposed to ice area, also resulted in better agreement between the model and observations when comparing the temporal evolution of ice. The larger discrepancies when using ice area as a metric suggests that it amplifies any model or observational deficiencies compared to when using ice extent. The use of cumulative ice area in the sensitivity experiments would therefore reveal a larger signal if any of the variables contribute to these model biases. The sensitivity experiments demonstrate that these biases are not easily removed or likely to change the minimum CFDD, at least by the variables tested here. Negligible differences in modelled and observed SSTs for the months leading up to ice formation suggests that the bias in ice evolution is dominated by model ice physics and atmospheric temperatures, as explored by the sensitivity experiments. Taking this into account, along with the emulation of model sea ice behaviour to observations in response to CFDD, the outcomes of the sensitivity experiments are likely to remain valid despite the bias present in the model. Only three years were simulated in the model due to the computationally intensive nature of the sensitivity experiments. However, the chosen years for the model sensitivities sample the extremes of past maximal ice extent, and temperatures within the historical range (Figure 9). Given the reasonable replication of observed sea ice behaviour in the control model, the simulated range of responses seen in the sensitivity experiments are likely to be representative of the historical observations.

The CFDD and cumulative ice area were found not to be significantly modified by differences in model ice albedo. This is in contrast to the Arctic, where analysis of its annual cycle shows that an increase in surface albedo from approximately 50 to 80% corresponds to a surface temperature drop of around 30°C (Curry *et al.* 1995). The key difference between the Arctic and the Caspian is likely to be the size of the ice area, so that local cooling feedbacks are overwhelmed by advection over the Caspian.

Ice compressive strength is also not a strong factor in determining the relationship between air temperature and sea ice. Some previous examples of the values postulated for compressive strength include 500, 5000, 15000, 27500 and 30000 Nm^{-2} (Hibler III and Walsh 1982; Kreyscher *et al.* 2000). This large range of possible values is thought to partly arise due to differences in regional surface wind stress (Tremblay and Hakakian 2006), and is unclear what the exact value should be for the Caspian. However, the exact value may not matter as the differences in compressive strength, which in turn varies ice coverage, only starts becoming significant in regions of more than 80 % fractional ice concentration (Leppäranta 2011). The daily correlations may be very weakly affected by differences in compressive strength given that ice concentrations of more than 80% only accounts for about 21% of the cumulative ice area in the Northern Caspian.

The modified sensitivity of cumulative ice area to air temperatures due to fluctuating sea levels may be attributed to changes in Caspian water volume and therefore its heat capacity. This has been the case for the increased sensitivity for ice formation in the neighbouring Aral Sea as sea levels decline (Kouraev *et al.* 2004). For the Caspian, this sensitivity appears to especially promote less heat content and enhanced closed ice formation for reduced sea levels. A 9m drop in Caspian Sea level may occur over the 21st century according to AOGCM ensemble averages of hydrologic budget estimates (Elguindi and Giorgi 2006). This change may delay the projected trend of an ice-free Caspian by 2100 for the high emission scenario in CMIP5.

5. Conclusion

Relationships between air temperatures and ice conditions in the Northern Caspian were found from historical observations. Correlations between an index of air temperatures based on stations around the Northern Caspian and cumulative area showed critical monthly mean temperatures between 5.5 and 9.5°C, and a minimum CFDD of 3.6±11.2°C, required for ice formation in the basin. These critical temperatures suggested that the Northern Caspian may be largely ice-free by 2100, based on climate projections of monthly mean air temperatures from multi-model ensembles. Modifications in the sensitivity of these correlations to differences in sea ice albedo, compressive strength and sea level were examined in a regional ocean-ice-atmosphere model. The model, which emulated observed sea ice conditions, showed weak sensitivities of the daily response of cumulative ice area evolution to CFDD, to differences in sea ice albedo and compressive strength. The model sensitivity studies suggest that the inference of a future ice free Caspian (based on empirical observations of temperature and sea ice) is robust in the sense it is unlikely to be affected by changes or uncertainties in ice albedo or compressive strength. However, less CFDD may be required for the onset of freezing if sea level reduces, in addition to closed ice formation being promoted. This may delay the projection of a largely ice-free Caspian.

Acknowledgement

With thanks to BP Environment Technology Programme and EPSRC. We acknowledge the World Climate Research Programme's Working Group on Coupled Modelling, which is responsible for CMIP, and we thank the climate modelling groups (which can be found at http://cmip-pcmdi.llnl.gov/cmip5/citation.html) for producing and making available their model output. For CMIP the U.S. Department of Energy's Program for Climate Model Diagnosis and Intercomparison provides coordinating support and led development of software infrastructure in partnership with the Global Organization for Earth System Science Portals.

References

Andreev O, Ivanov B. 2012. The use of one-dimensional thermodynamic model for computing the level ice thickness and hummock freezing intensity in the northern caspian sea. *Russian Meteorology and Hydrology* **37**(1): 34–38.

Arpe K, Bengtsson L, Golitsyn G, Mokhov I, Semenov V, Sporyshev P. 2000. Connection between caspian sea level variability and enso. *Geophysical research letters* **27**(17): 2693–2696.

Assel RA. 1980. Maximum freezing degree-days as a winter severity index for the great lakes, 1897–1977. *Monthly Weather Review* **108**(9): 1440–1445.

Assel RA. 1991. Implications of co2 global warming on great lakes ice cover. *Climatic Change* **18**(4): 377–395.

Assel RA, Janowiak JE, Young S, Boyce D. 1996. Winter 1994 weather and ice conditions for the laurentian great lakes. *Bulletin of the American Meteorological Society* **77**(1): 71–88.

Bailey E, Feltham D, Sammonds P. 2010. A model for the consolidation of rafted sea ice. *Journal of Geophysical Research: Oceans (1978–2012)* **115**(C4).

Barry R, Gan TY. 2011. *The global cryosphere: past, present and future*. Cambridge University Press.

Budgell W. 2005. Numerical simulation of ice-ocean variability in the barents sea region. *Ocean Dynamics* **55**(3-4): 370–387.

Business B. 2002. *Ice engineering*. University Press of the Pacific, ISBN 9780898758443.

Cavalieri DJ, Parkinson CL, Gloersen P, Comiso JC, Zwally HJ. 1999. Deriving long-term time series of sea ice cover from satellite passive-microwave multisensor data sets.

Journal of Geophysical Research: Oceans (1978–2012) **104**(C7): 15 803–15 814.

Curry JA, Schramm JL, Ebert EE. 1995. Sea ice-albedo climate feedback mechanism. *Journal of Climate* **8**(2): 240–247.

Danielson S, Curchitser E, Hedstrom K, Weingartner T, Stabeno P. 2011. On ocean and sea ice modes of variability in the bering sea. *Journal of Geophysical Research: Oceans (1978–2012)* **116**(C12).

Dee D, Uppala S, Simmons A, Berrisford P, Poli P, Kobayashi S, Andrae U, Balmaseda M, Balsamo G, Bauer P, *et al.* 2011. The era-interim reanalysis: Configuration and performance of the data assimilation system. *Quarterly Journal of the Royal Meteorological Society* **137**(656): 553–597.

Elguindi N, Giorgi F. 2006. Projected changes in the caspian sea level for the 21st century based on the latest aogcm simulations. *Geophysical research letters* **33**(8).

Elguindi N, Giorgi F. 2007. Simulating future caspian sea level changes using regional climate model outputs. *Climate dynamics* **28**(4): 365–379.

EUMETSAT Ocean and Sea Ice Satellite Application Facility. 2011. Global sea ice concentration reprocessing dataset 1978-2009 (v1.1, 2011), [online]. *Norwegian and Danish Meteorological Institutes* .

Falk-Petersen S, Hop H, Budgell WP, Hegseth EN, Korsnes R, Løyning TB, Børre Ørbæk J, Kawamura T, Shirasawa K. 2000. Physical and ecological processes in the marginal ice zone of the northern barents sea during the summer melt period. *Journal of Marine Systems* **27**(1): 131–159.

Farmer GT, Cook J. 2013. *Climate change science: A modern synthesis: Volume 1-the physical climate*, vol. 1. Springer.

Frolov A, Asmus V, Zemlyanov I, Zilbershtein O, Krovotyntsev V, Martyshchenko V, Mironov E. 2009. Complex studies of hydrometeorological and ice conditions on the northwestern shelf of the caspian sea based on satellite and expedition observational data and model calculations. *Russian Meteorology and Hydrology* **34**(3): 148–158.

Gloersen P, Campbell WJ, Cavalieri DJ, Comiso JC, Parkinson CL, Zwally HJ, *et al.* 1992. Arctic and antarctic sea ice, 1978-1987: Satellite passive-microwave observations and analysis .

Haidvogel DB, Arango HG, Hedstrom K, Beckmann A, Malanotte-Rizzoli P, Shchepetkin AF. 2000. Model evaluation experiments in the north atlantic basin: simulations in nonlinear terrain-following coordinates. *Dynamics of Atmospheres and Oceans* **32**(3): 239–281.

Hall D, Salomonson VV, Riggs GA. 2006. Modis/terra snow cover daily l3 global 500m grid. *Boulder, Colorado USA: National Snow and Ice Data Center* **Version 5**(MOD10A1).

Hibler III W. 1979. A dynamic thermodynamic sea ice model. *Journal of Physical Oceanography* **9**(4): 815–846.

Hibler III WD, Walsh JE. 1982. On modeling seasonal and interannual fluctuations of arctic sea ice. *Journal of Physical Oceanography* **12**: 1514–1523.

Hunke E, Dukowicz J. 1997. An elastic-viscous-plastic model for sea ice dynamics. *Journal of Physical Oceanography* **27**(9): 1849–1867.

Ibrayev R, Özsoy E, Schrum C, Sur H. 2009. Seasonal variability of the caspian sea three-dimensional circulation, sea level and air-sea interaction. *Ocean Science Discussions* **6**: 1913–1970.

Kitazawa D, Yang J. 2012. Numerical analysis of water circulation and thermohaline structures in the caspian sea. *Journal of Marine Science and Technology* **17**(2): 168–180.

Klein Tank A, Wijngaard J, Können G, Böhm R, Demarée G, Gocheva A, Mileta M, Pashiardis S, Hejkrlik L, Kern-Hansen C, *et al.* 2002. Daily dataset of 20th-century surface air temperature and precipitation series for the european climate assessment. *International Journal of*

Climatology **22**(12): 1441–1453.

Klyachkin S. 2011. Estimates of intensity and formation frequency of ice pile-up on the northwestern coast of the caspian sea from the results of model computations. *Russian Meteorology and Hydrology* **36**(3): 193–199.

Kouraev AV, Papa F, Mognard NM, Buharizin PI, Cazenave A, Cretaux JF, Dozortseva J, Remy F. 2004. Sea ice cover in the caspian and aral seas from historical and satellite data. *Journal of marine systems* **47**(1): 89–100.

Kreyscher M, Harder M, Lemke P, Flato GM. 2000. Results of the sea ice model intercomparison project: Evaluation of sea ice rheology schemes for use in climate simulations. *Journal of Geophysical Research: Oceans (1978–2012)* **105**(C5): 11 299–11 320.

Leppäranta M. 2011. *The drift of sea ice*. Springerverlag Berlin Heidelberg.

Lofgren BM, Quinn FH, Clites AH, Assel RA, Eberhardt AJ, Luukkonen CL. 2002. Evaluation of potential impacts on great lakes water resources based on climate scenarios of two gcms. *Journal of Great Lakes Research* **28**(4): 537–554.

MacCallum SN, Merchant CJ. 2013. Arc-lake v2.0, 1991-2011 alid0001. *University of Edinburgh, School of GeoSciences / European Space Agency* .

Maykut GA. 1978. Energy exchange over young sea ice in the central arctic. *Journal of Geophysical Research: Oceans (1978–2012)* **83**(C7): 3646–3658.

Mellor GL, Kantha L. 1989. An ice-ocean coupled model. *Journal of Geophysical Research: Oceans (1978–2012)* **94**(C8): 10 937–10 954.

National Ice Centre. 2008. Ims daily northern hemisphere snow and ice analysis at 4 km and 24 km resolution. 1january2006 to 31december2009. *Boulder, Colorado USA: National Snow and Ice Data Center* .

Parkinson CL, Cavalieri DJ, Gloersen P, Zwally HJ, Comiso JC. 1999. Arctic sea ice extents, areas, and trends, 1978–1996. *Journal of Geophysical Research: Oceans (1978–2012)* **104**(C9): 20 837–20 856.

Renssen H, Lougheed B, Aerts J, De Moel H, Ward P, Kwadijk J. 2007. Simulating long-term caspian sea level changes: the impact of holocene and future climate conditions. *Earth and Planetary Science Letters* **261**(3): 685–693.

Rodionov SN. 1994. *Global and regional climate interaction: the caspian sea experience*, vol. 11. Springer.

Semenov V, Mokhov I, Latif M. 2012. Influence of the ocean surface temperature and sea ice concentration on regional climate changes in eurasia in recent decades. *Izvestiya, Atmospheric and Oceanic Physics* **48**(4): 355–372.

Shchepetkin AF, McWilliams JC. 2005. The regional oceanic modeling system (roms): a split-explicit, free-surface, topography-following-coordinate oceanic model. *Ocean Modelling* **9**(4): 347–404.

Skamarock W, Klemp J, Dudhia J, Gill D, Barker D, Duda M, Huang X, Wang W, Powers J. 2008. A description of the advanced research wrf version 3, ncar technical note. Technical report, NCAR/TN–475+ STR.

Stark JD, Donlon CJ, Martin MJ, McCulloch ME. 2007. Ostia: An operational, high resolution, real time, global sea surface temperature analysis system. In: *Oceans 2007-Europe*. IEEE, pp. 1–4.

Su H, Wang Y, Yang J. 2012. Monitoring the spatiotemporal evolution of sea ice in the bohai sea in the 2009–2010 winter combining modis and meteorological data. *Estuaries and coasts* **35**(1): 281–291.

Syed FS, Giorgi F, Pal J, Keay K. 2010. Regional climate model simulation of winter climate over central–southwest asia, with emphasis on nao and enso effects. *International Journal of Climatology* **30**(2): 220–235.

Taylor KE, Stouffer RJ, Meehl GA. 2012. An overview of cmip5 and the experiment design. *Bulletin of the American Meteorological Society* **93**(4).

Thomas D, Dieckmann G. 2008. *Sea ice: An introduction to its physics, chemistry, biology and geology*. Wiley, ISBN 9780470756928.

Climatology **22**(12): 1441–1453.

Klyachkin S. 2011. Estimates of intensity and formation frequency of ice pile-up on the northwestern coast of the caspian sea from the results of model computations. *Russian Meteorology and Hydrology* **36**(3): 193–199.

Kouraev AV, Papa F, Mognard NM, Buharizin PI, Cazenave A, Cretaux JF, Dozortseva J, Remy F. 2004. Sea ice cover in the caspian and aral seas from historical and satellite data. *Journal of marine systems* **47**(1): 89–100.

Kreyscher M, Harder M, Lemke P, Flato GM. 2000. Results of the sea ice model intercomparison project: Evaluation of sea ice rheology schemes for use in climate simulations. *Journal of Geophysical Research: Oceans (1978–2012)* **105**(C5): 11 299–11 320.

Leppäranta M. 2011. *The drift of sea ice*. Springerverlag Berlin Heidelberg.

Lofgren BM, Quinn FH, Clites AH, Assel RA, Eberhardt AJ, Luukkonen CL. 2002. Evaluation of potential impacts on great lakes water resources based on climate scenarios of two gcms. *Journal of Great Lakes Research* **28**(4): 537–554.

MacCallum SN, Merchant CJ. 2013. Arc-lake v2.0, 1991-2011 alid0001. *University of Edinburgh, School of GeoSciences / European Space Agency* .

Maykut GA. 1978. Energy exchange over young sea ice in the central arctic. *Journal of Geophysical Research: Oceans (1978–2012)* **83**(C7): 3646–3658.

Mellor GL, Kantha L. 1989. An ice-ocean coupled model. *Journal of Geophysical Research: Oceans (1978–2012)* **94**(C8): 10 937–10 954.

National Ice Centre. 2008. Ims daily northern hemisphere snow and ice analysis at 4 km and 24 km resolution. 1january2006 to 31december2009. *Boulder, Colorado USA: National Snow and Ice Data Center* .

Parkinson CL, Cavalieri DJ, Gloersen P, Zwally HJ, Comiso JC. 1999. Arctic sea ice extents, areas, and trends, 1978–1996. *Journal of Geophysical Research: Oceans (1978–2012)* **104**(C9): 20 837–20 856.

Renssen H, Lougheed B, Aerts J, De Moel H, Ward P, Kwadijk J. 2007. Simulating long-term caspian sea level changes: the impact of holocene and future climate conditions. *Earth and Planetary Science Letters* **261**(3): 685–693.

Rodionov SN. 1994. *Global and regional climate interaction: the caspian sea experience*, vol. 11. Springer.

Semenov V, Mokhov I, Latif M. 2012. Influence of the ocean surface temperature and sea ice concentration on regional climate changes in eurasia in recent decades. *Izvestiya, Atmospheric and Oceanic Physics* **48**(4): 355–372.

Shchepetkin AF, McWilliams JC. 2005. The regional oceanic modeling system (roms): a split-explicit, free-surface, topography-following-coordinate oceanic model. *Ocean Modelling* **9**(4): 347–404.

Skamarock W, Klemp J, Dudhia J, Gill D, Barker D, Duda M, Huang X, Wang W, Powers J. 2008. A description of the advanced research wrf version 3, ncar technical note. Technical report, NCAR/TN–475+ STR.

Stark JD, Donlon CJ, Martin MJ, McCulloch ME. 2007. Ostia: An operational, high resolution, real time, global sea surface temperature analysis system. In: *Oceans 2007-Europe*. IEEE, pp. 1–4.

Su H, Wang Y, Yang J. 2012. Monitoring the spatiotemporal evolution of sea ice in the bohai sea in the 2009–2010 winter combining modis and meteorological data. *Estuaries and coasts* **35**(1): 281–291.

Syed FS, Giorgi F, Pal J, Keay K. 2010. Regional climate model simulation of winter climate over central–southwest asia, with emphasis on nao and enso effects. *International Journal of Climatology* **30**(2): 220–235.

Taylor KE, Stouffer RJ, Meehl GA. 2012. An overview of cmip5 and the experiment design. *Bulletin of the American Meteorological Society* **93**(4).

Thomas D, Dieckmann G. 2008. *Sea ice: An introduction to its physics, chemistry, biology and geology*. Wiley, ISBN 9780470756928.